

# Search for a pentaquark decaying to $pK_S^0$

The FOCUS Collaboration <sup>1</sup>

J. M. Link <sup>a</sup> P. M. Yager <sup>a</sup> J. C. Anjos <sup>b</sup> I. Bediaga <sup>b</sup>  
 C. Castromonte <sup>b</sup> A. A. Machado <sup>b</sup> J. Magnin <sup>b</sup> A. Massafferri <sup>b</sup>  
 J. M. de Miranda <sup>b</sup> I. M. Pepe <sup>b</sup> E. Polycarpo <sup>b</sup> A. C. dos Reis <sup>b</sup>  
 S. Carrillo <sup>c</sup> E. Casimiro <sup>c</sup> E. Cuautle <sup>c</sup> A. Sánchez-Hernández <sup>c</sup>  
 C. Uribe <sup>c</sup> F. Vázquez <sup>c</sup> L. Agostino <sup>d</sup> L. Cinquini <sup>d</sup>  
 J. P. Cumalat <sup>d</sup> V. Frisullo <sup>d</sup> B. O'Reilly <sup>d</sup> I. Segoni <sup>d</sup>  
 K. Stenson <sup>d</sup> J. N. Butler <sup>e</sup> H. W. K. Cheung <sup>e</sup> G. Chiodini <sup>e</sup>  
 I. Gaines <sup>e</sup> P. H. Garbincius <sup>e</sup> L. A. Garren <sup>e</sup> E. Gottschalk <sup>e</sup>  
 P. H. Kasper <sup>e</sup> A. E. Kreymer <sup>e</sup> R. Kutschke <sup>e</sup> M. Wang <sup>e</sup>  
 L. Benussi <sup>f</sup> M. Bertani <sup>f</sup> S. Bianco <sup>f</sup> F. L. Fabbri <sup>f</sup> S. Pacetti <sup>f</sup>  
 A. Zallo <sup>f</sup> M. Reyes <sup>g</sup> C. Cawfield <sup>h</sup> D. Y. Kim <sup>h</sup> A. Rahimi <sup>h</sup>  
 J. Wiss <sup>h</sup> R. Gardner <sup>i</sup> A. Kryemadhi <sup>i</sup> Y. S. Chung <sup>j</sup> J. S. Kang <sup>j</sup>  
 B. R. Ko <sup>j</sup> J. W. Kwak <sup>j</sup> K. B. Lee <sup>j</sup> K. Cho <sup>k</sup> H. Park <sup>k</sup>  
 G. Alimonti <sup>l</sup> S. Barberis <sup>l</sup> M. Boschini <sup>l</sup> A. Cerutti <sup>l</sup>  
 P. D'Angelo <sup>l</sup> M. DiCorato <sup>l</sup> P. Dini <sup>l</sup> L. Edera <sup>l</sup> S. Erba <sup>l</sup>  
 P. Inzani <sup>l</sup> F. Leveraro <sup>l</sup> S. Malvezzi <sup>l</sup> D. Menasce <sup>l</sup>  
 M. Mezzadri <sup>l</sup> L. Moroni <sup>l</sup> D. Pedrini <sup>l</sup> C. Pontoglio <sup>l</sup> F. Prelz <sup>l</sup>  
 M. Rovere <sup>l</sup> S. Sala <sup>l</sup> T. F. Davenport III <sup>m</sup> V. Arena <sup>n</sup> G. Boca <sup>n</sup>  
 G. Bonomi <sup>n</sup> G. Gianini <sup>n</sup> G. Liguori <sup>n</sup> D. Lopes Pegna <sup>n</sup>  
 M. M. Merlo <sup>n</sup> D. Pantea <sup>n</sup> S. P. Ratti <sup>n</sup> C. Riccardi <sup>n</sup> P. Vitulo <sup>n</sup>  
 C. Göbel <sup>o</sup> J. Olatoro <sup>o</sup> H. Hernandez <sup>p</sup> A. M. Lopez <sup>p</sup>  
 H. Mendez <sup>p</sup> A. Paris <sup>p</sup> J. Quinones <sup>p</sup> J. E. Ramirez <sup>p</sup> Y. Zhang <sup>p</sup>  
 J. R. Wilson <sup>q</sup> T. Handler <sup>r</sup> R. Mitchell <sup>r</sup> D. Engh <sup>s</sup>  
 K. M. Givens <sup>s</sup> M. Hosack <sup>s</sup> W. E. Johns <sup>s</sup> E. Luiggi <sup>s</sup>  
 M. Nehring <sup>s</sup> P. D. Sheldon <sup>s</sup> E. W. Vaandering <sup>s</sup> M. Webster <sup>s</sup>  
 M. Sheaff <sup>t</sup>

<sup>a</sup>University of California, Davis, CA 95616

<sup>b</sup>Centro Brasileiro de Pesquisas Físicas, Rio de Janeiro, RJ, Brazil

<sup>c</sup>CINVESTAV, 07000 México City, DF, Mexico

<sup>d</sup>*University of Colorado, Boulder, CO 80309*  
<sup>e</sup>*Fermi National Accelerator Laboratory, Batavia, IL 60510*  
<sup>f</sup>*Laboratori Nazionali di Frascati dell'INFN, Frascati, Italy I-00044*  
<sup>g</sup>*University of Guanajuato, 37150 Leon, Guanajuato, Mexico*  
<sup>h</sup>*University of Illinois, Urbana-Champaign, IL 61801*  
<sup>i</sup>*Indiana University, Bloomington, IN 47405*  
<sup>j</sup>*Korea University, Seoul, Korea 136-701*  
<sup>k</sup>*Kyungpook National University, Taegu, Korea 702-701*  
<sup>l</sup>*INFN and University of Milano, Milano, Italy*  
<sup>m</sup>*University of North Carolina, Asheville, NC 28804*  
<sup>n</sup>*Dipartimento di Fisica Nucleare e Teorica and INFN, Pavia, Italy*  
<sup>o</sup>*Pontifícia Universidade Católica, Rio de Janeiro, RJ, Brazil*  
<sup>p</sup>*University of Puerto Rico, Mayaguez, PR 00681*  
<sup>q</sup>*University of South Carolina, Columbia, SC 29208*  
<sup>r</sup>*University of Tennessee, Knoxville, TN 37996*  
<sup>s</sup>*Vanderbilt University, Nashville, TN 37235*  
<sup>t</sup>*University of Wisconsin, Madison, WI 53706*

---

## Abstract

We present a search for a pentaquark decaying strongly to  $pK_S^0$  in  $\gamma N$  collisions at a center-of-mass energy up to 25 GeV/ $c^2$ . Finding no evidence for such a state in the mass range of 1470 MeV/ $c^2$  to 2200 MeV/ $c^2$ , we set limits on the yield and on the cross section times branching ratio relative to  $\Sigma^*(1385)^\pm$  and  $K^*(892)^\pm$ .

*Key words:*

*PACS:* 14.80.-j 13.60.Le 13.60.Rj

---

## 1 Introduction

Nearly 30 years ago Jaffe proposed the existence of bound (mass below threshold for strong decay) multiquark states including  $Q\bar{Q}q\bar{q}$  states and the  $H$  dihyperon [1] based on calculations using the bag model [2]. As the years passed and no convincing evidence for non mesonic and non baryonic states was found the field languished.

---

<sup>1</sup> See <http://www-focus.fnal.gov/authors.html> for additional author information.

Between January 2003 and March 2004, however, the pentaquark field was reenergized when no less than ten independent pentaquark observations at a mass around  $1540 \text{ MeV}/c^2$  were reported [3,4,5,6,7,8,9,10,11,12]. The presumed quark content of the reported states was  $(\bar{s}uudd)$ . The reported widths were consistent with detector resolution even though a strong decay is allowed. Even more amazing was the prediction six years before by Diakonov *et al.* of just such a state at a mass around  $1530 \text{ MeV}/c^2$  and a width less than  $15 \text{ MeV}/c^2$  [13]. Observations of a doubly-strange pentaquark [14] and a charm pentaquark [15] have also been reported by single experiments.

The original observations were made in the  $nK^+$  mode. For a state to decay strongly to  $nK^+$ , it must be composed of at least 5 quarks. Other observations have been made in the  $pK_S^0$  mode which is not manifestly exotic since the  $K_S^0$  can originate from a  $K^0$  or  $\bar{K}^0$ ; a  $p\bar{K}^0$  decay is not exotic while a  $pK^0$  decay is exotic. Since that time, many other experiments have failed to find evidence of pentaquarks [16,17,18,19,20,21,22,23,24,25,26]. Most of these experiments are higher statistics and higher energy than the observing experiments and generally search the  $pK_S^0$  decay mode. Recently CLAS, which previously reported two observations failed to find pentaquarks in a third attempt [27]. This letter presents a search of the FOCUS data for the  $\Theta^+(\bar{s}uudd)$  pentaquark candidate in the decay mode  $\Theta^+ \rightarrow pK_S^0$ . Cross sections will be measured relative to three well known states with a similar decay topology:  $\Sigma^*(1385)^\pm \rightarrow \Lambda^0\pi^\pm$  (two states) and  $K^*(892)^+ \rightarrow K_S^0\pi^+$ <sup>2</sup>.

## 2 Event reconstruction and selection

The FOCUS experiment recorded data during the 1996–7 fixed-target run at Fermilab. A photon beam obtained from bremsstrahlung of 300 GeV electrons and positrons impinged on a set of BeO targets. Four sets of silicon strip detectors, each with three views, were located downstream of the targets for vertexing and track finding. For most of the run, two pairs of silicon strips were also interleaved with the target segments for more precise vertexing [28]. Charged particles were tracked and momentum analyzed as they passed through one or two dipole magnets and three to five sets of multi-wire proportional chambers with four views each. Three multicell threshold Čerenkov counters, two electromagnetic calorimeters, and two muon detectors provided particle identification. A trigger which required, among other things,  $\gtrsim 25 \text{ GeV}$  of hadronic energy passed 6 billion events for reconstruction.

The data used for this analysis come from a subset of FOCUS data which contain vee candidates ( $K_S^0 \rightarrow \pi^+\pi^-$  and  $\Lambda^0 \rightarrow p\pi^-$ ). There are four vee candidate

---

<sup>2</sup> Charged conjugate states are implied unless explicitly stated otherwise

types which are used in this analysis. SSD vees decay in the vertex region and have decay tracks which are found in the silicon system. Magnet vees decay further downstream and tracks are reconstructed in the wire chambers. The magnet vees are divided into three types SS, TS, TT for stub-stub, track-stub, and track-track depending on whether the decay particles are tracked in only the upstream 3 wire chambers (stubs) or in all 5 wire chambers (tracks). A full description of vee reconstruction in FOCUS can be found in Ref. [29].

The vee selection requires a reconstructed vee vertex with some quality, particle identification, and mass cuts. The quality requirements include good track quality, a good vertex for the two tracks, and a minimum vee momentum of 5 GeV/ $c$ . The mass requirement for a  $K_S^0$  candidate is to have a normalized mass within 4 (5)  $\sigma$  of the nominal mass for SSD (magnet) vees. The  $\Lambda^0$  mass requirement is for the invariant mass to be between 1.09 GeV/ $c^2$  and 1.14 GeV/ $c^2$ . The particle identification cuts on the vee daughters use the FOCUS Čerenkov identification algorithm [30]. This algorithm returns negative log-likelihood (times two) values  $\mathcal{W}_i(j)$  for track  $j$  and hypothesis  $i \in \{e, \pi, K, p\}$  based on the light yields in the phototubes covering the Čerenkov cone of the track. The information from all three Čerenkov detectors is combined. The vee daughter pion candidates must not be strongly inconsistent with the pion hypothesis:  $\mathcal{W}_{\min}(\pi) - \mathcal{W}_\pi(\pi) > -5$  where  $\mathcal{W}_{\min}$  is the minimum of the four hypotheses. The small phase space of the  $\Lambda^0 \rightarrow p\pi^-$  decay and the forward nature of the FOCUS spectrometer require the proton to have a higher lab momentum than the pion. Thus, the higher momentum track is chosen to be the proton and it must have  $\mathcal{W}_{\min}(p) - \mathcal{W}_p(p) > -5$  and  $\mathcal{W}_\pi(p) - \mathcal{W}_p(p) > 1$ . To reduce combinatorics, the event is only kept if the number of vees passing the above cuts was no more than two. At least one and no more than seven good quality charged tracks with momentum greater than 5 GeV/ $c$  must be found in addition to the vee(s). These tracks and any SSD vees must be consistent with originating from a single vertex with confidence level greater than 1%. The total number of good quality vees plus good quality charged tracks must exceed two. After applying all of the above cuts, the vee sample within  $3\sigma$  of the nominal mass is selected which contains 72 million  $K_S^0 \rightarrow \pi^+\pi^-$  (9 million  $\Lambda^0 \rightarrow p\pi^-$ ) candidates of which 90% (95%) are signal as shown in Fig. 1. Each vee in an event is combined with the good quality charged tracks in the event to search for  $K^*(892)^+ \rightarrow K_S^0\pi^+$ ,  $\Sigma^*(1385)^\pm \rightarrow \Lambda^0\pi^\pm$ , and  $\Theta^+ \rightarrow pK_S^0$ . The Čerenkov requirements on the charged tracks are  $\mathcal{W}_{\min}(\pi) - \mathcal{W}_\pi(\pi) > -2$  for pions plus  $\mathcal{W}_K(\pi) - \mathcal{W}_\pi(\pi) > 1$  for the pion from the  $\Sigma^*(1385)^\pm$  decay. The proton from the  $\Theta^+$  decay must have  $\mathcal{W}_\pi(p) - \mathcal{W}_p(p) > 8$  and  $\mathcal{W}_K(p) - \mathcal{W}_p(p) > 3$ .

The  $K_S^0\pi^+$  and  $\Lambda^0\pi^\pm$  are shown in Figs. 2 and 3, respectively. In both cases, the signal was best fit with an S-wave Breit-Wigner with an energy independent width even though a P-wave energy dependent width would be more appropriate. The Breit-Wigner was convoluted with a Gaussian for the detector res-

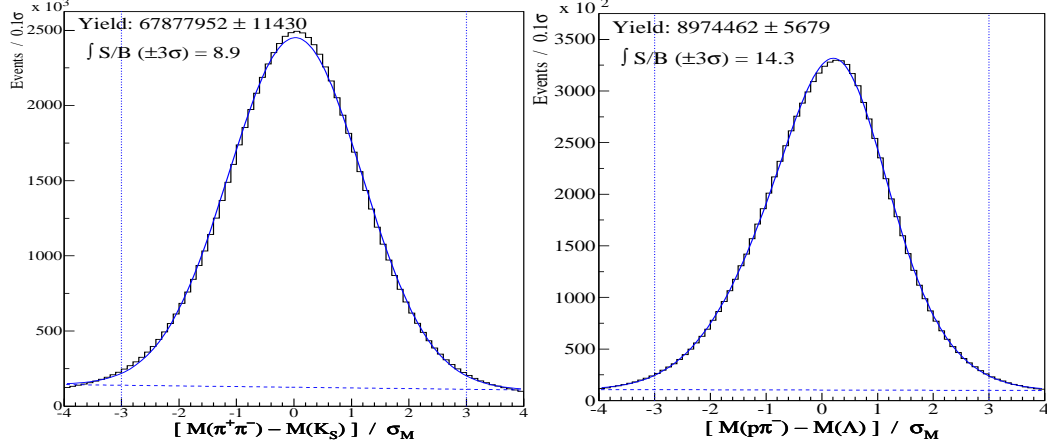


Fig. 1. The normalized mass plots of  $K_S^0 \rightarrow \pi^+\pi^-$  and  $\Lambda^0 \rightarrow p^-\pi^-$  candidates. Events inside the vertical lines are selected for analysis.

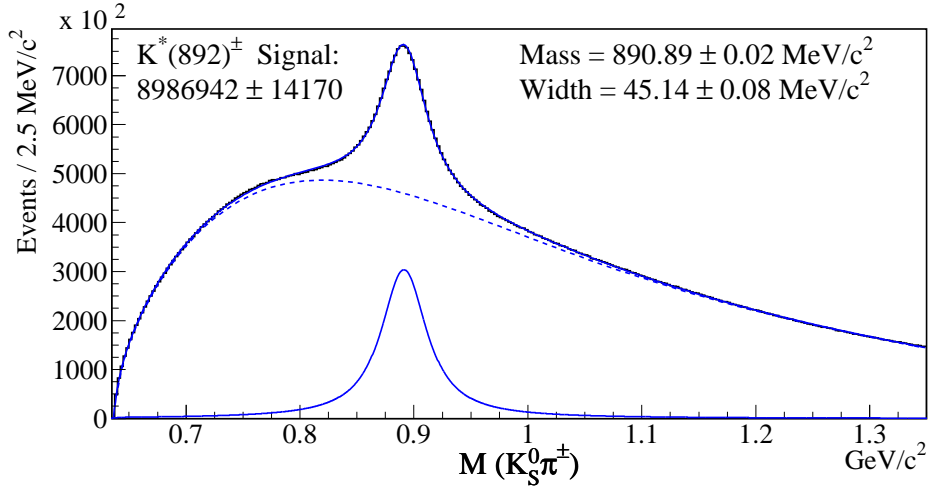


Fig. 2.  $K^*(892)^+$  fit with an S-wave Breit-Wigner and combinatorial background.

olution obtained from a Monte Carlo simulation. The  $K^*(892)^+$ ,  $\Sigma^*(1385)^+$ , and  $\Sigma^*(1385)^-$  resolutions are  $5.1 \text{ MeV}/c^2$ ,  $3.2 \text{ MeV}/c^2$ , and  $3.2 \text{ MeV}/c^2$ . The background was fit to the form  $aq^b \exp(cq + dq^2 + eq^3 + fq^4)$  where  $a$ – $f$  are free parameters and  $q$  is the  $Q$ -value (invariant mass minus component masses).

### 3 Pentaquark search results

The  $pK_S^0$  and  $\bar{p}K_S^0$  invariant masses are plotted using the standard selection criteria in Fig. 4. There are no significant differences between the two charge states so for the remainder of the analysis we combine the charge conjugate states. The combined sample with standard cuts and with an additional momentum asymmetry cut is plotted in Fig. 5. The momentum asymmetry cut,

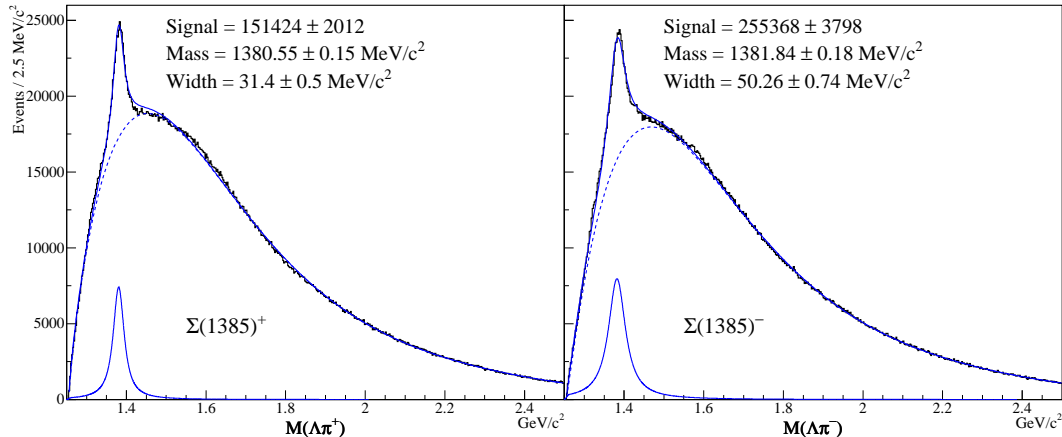


Fig. 3.  $\Sigma^*(1385)^\pm$  fits with an S-wave Breit-Wigner and combinatorial background.

requiring the proton to have a higher momentum than the  $K_S^0$  in the pentaquark decay, has been suggested as a method of reducing background. The true effect of the cut is to sculpt the mass distribution into a more peaked structure near the location of the previously observed pentaquarks and is not used in the analysis. In Fig. 6 the total sample is fit to a background curve of the form  $aq^b \exp(cq + dq^2 + eq^3 + fq^4)$  where  $a$ – $f$  are free parameters and  $q$  is the  $Q$ -value:  $q \equiv M(pK_S^0) - m_p - m_{K^0}$ . No evidence for a pentaquark near 1540  $\text{MeV}/c^2$  or at any mass less than 2400  $\text{MeV}/c^2$  is observed. To set a limit on the yield we need to make some assumptions about the width of the state. We consider two cases: one with a natural width of 0 and one with a natural width of 15  $\text{MeV}/c^2$ . In the first case, the signal is fit with a Gaussian with a width set by the experimental resolution. In the second case, the signal is fit with an S-wave Breit-Wigner with an energy independent width convoluted with the experimental resolution. The experimental resolution in  $\text{MeV}/c^2$  is approximately  $\sigma(\text{MeV}/c^2) = -22.5 + 19.48m - 1.99m^2$  where  $m$  is the mass in  $\text{GeV}/c^2$ .

A series of 731 fits to the observed  $pK_S^0$  mass plot were performed using the background and signal shapes described above. The signal mass is varied in 1  $\text{MeV}/c^2$  steps from 1470 to 2200  $\text{MeV}/c^2$  and a binned log-likelihood fit using MINUIT [31] is performed. The  $\pm 1\sigma$  errors are defined as the point where  $\Delta \log \mathcal{L} = 0.50$  relative to the maximum  $\log \mathcal{L}$ , while continually adjusting the background parameters to maximize  $\log \mathcal{L}$ . The 95% CL lower limit is defined similarly with  $\Delta \log \mathcal{L} = 1.92$ . Both are obtained using MINOS [31]. The 95% CL upper limit is constructed as follows: The likelihood function  $\mathcal{L}$  versus yield is determined by maximizing  $\log \mathcal{L}$  for many different (fixed) yields, allowing background parameters to float. The likelihood function is integrated from a yield of 0 to  $\infty$  to obtain the total likelihood. The 95% CL upper limit on the yield is defined as the point where 95% of the total likelihood is between a yield of 0 and the upper limit. The fitted yield, 1- $\sigma$  errors, and 95% CL limits are shown in Fig. 7. Of the 1462 fits, none of them finds a positive excursion

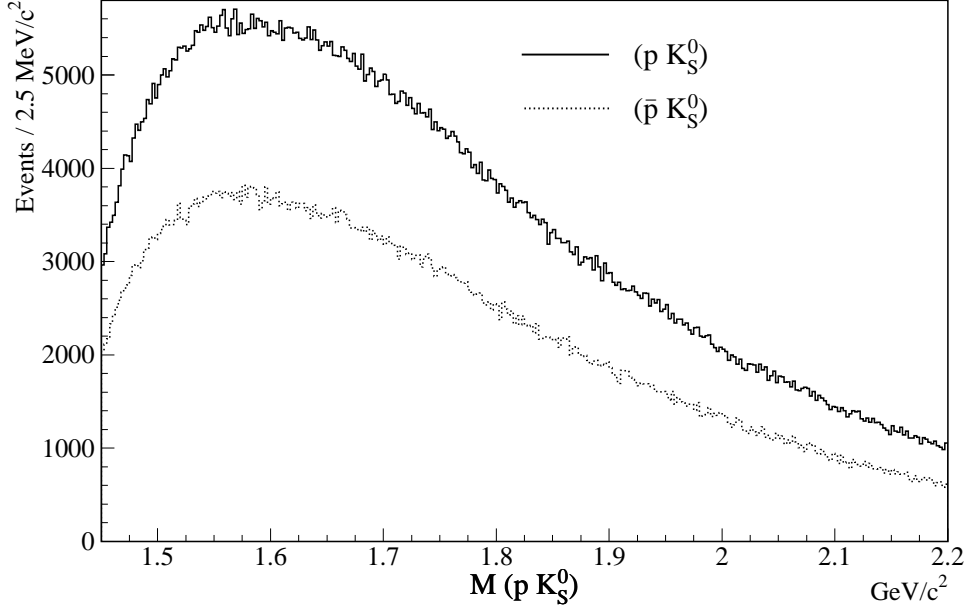


Fig. 4. Invariant mass distribution of  $pK_S^0$  separated by charge. Standard cuts are applied.

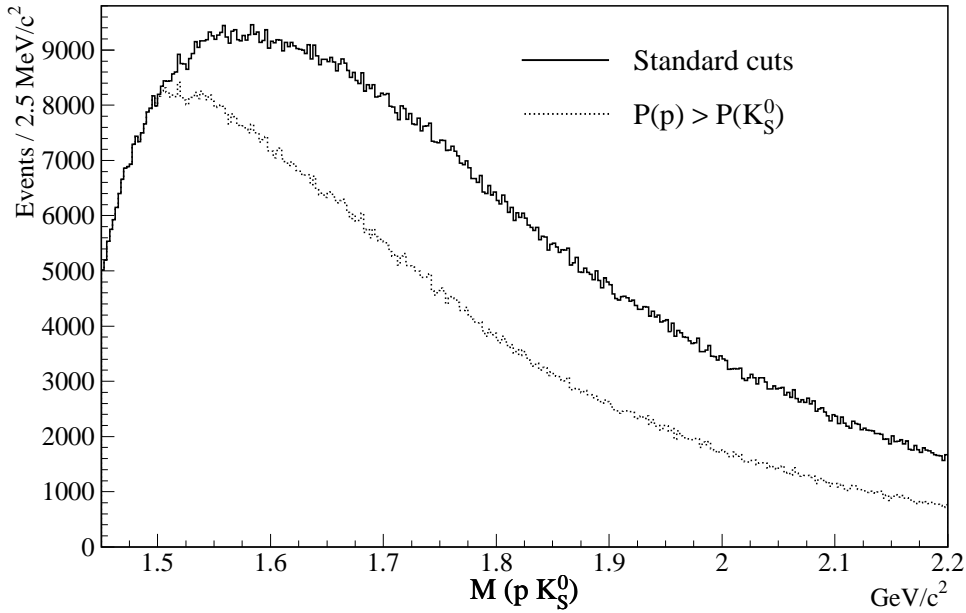


Fig. 5. Invariant mass distribution of  $pK_S^0$  for both charge states. Solid histogram shows the result for standard cuts and the dashed histogram is with an additional cut requiring the proton momentum be greater than the  $K_S^0$  momentum.

greater than  $5\sigma$ . Previous pentaquark observations have occurred between  $1520 \text{ MeV}/c^2$  and  $1555 \text{ MeV}/c^2$  with a very small natural width. In this region the largest excess we find is a  $2.5\sigma$  excess at  $1545 \text{ MeV}/c^2$  for the  $\Gamma = 0 \text{ MeV}/c^2$  fits. A  $3.1\sigma$  excess is seen at the same location for the  $\Gamma = 15 \text{ MeV}/c^2$  but this width would be inconsistent with the previous observations and is certainly not a convincing observation. Additionally, this excess occurs in a region where

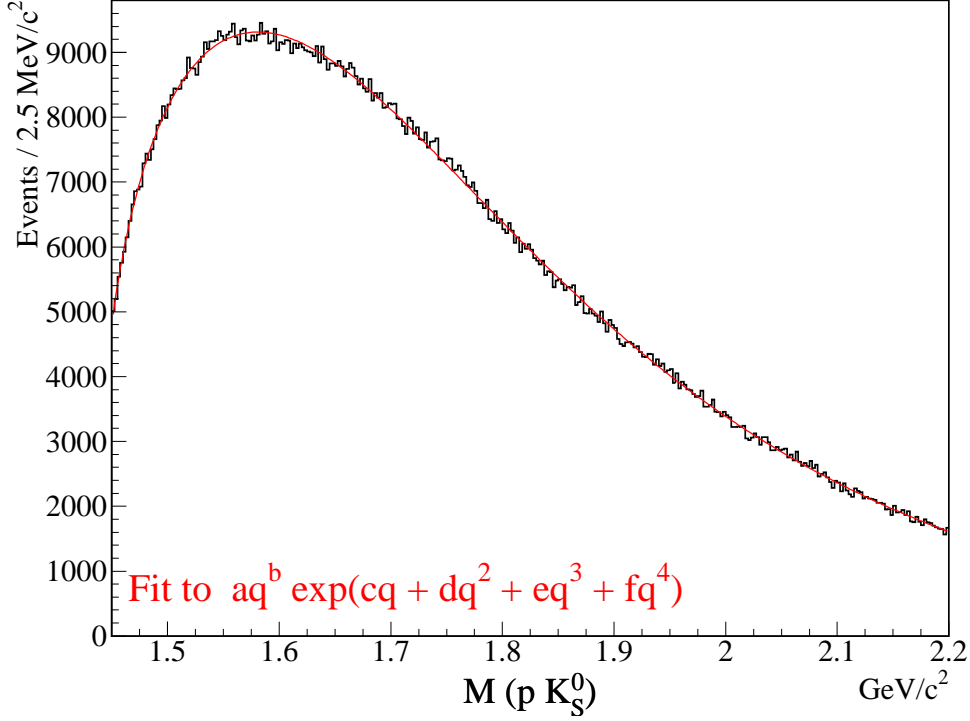


Fig. 6. Invariant mass distribution of  $pK_S^0$  for both charge states with standard cuts.

the background distribution is peaking which can give the appearance of a signal. Given the large number of fits, the appearance of 2–3 $\sigma$  excesses is not unlikely.

To compare with other experiments, the limits on yield must be converted to limits on production times (unknown) branching ratio. We choose to normalize the  $\Theta^+$  production cross section to  $\Sigma^*(1385)^\pm$  and  $K^*(892)^+$  because the reconstructed decay modes of these particles  $\Sigma^*(1385)^\pm \rightarrow \Lambda^0\pi^\pm$  and  $K^*(892)^+ \rightarrow K_S^0\pi^+$  are very similar, in terms of topology and energy release, to the signal. Thus, we attempt to determine

$$\frac{\sigma(\Theta^+) \cdot \text{BR}(\Theta^+ \rightarrow pK_S^0)}{\sigma(K^*(892)^+)} \quad \text{and} \quad \frac{\sigma(\Theta^+) \cdot \text{BR}(\Theta^+ \rightarrow pK_S^0)}{\sigma(\Sigma^*(1385)^\pm)}. \quad (1)$$

Rewriting Eq. 1 in terms of measured yields ( $Y$ ) and efficiencies ( $\epsilon$ ), we find:

$$\begin{aligned} \frac{\sigma(\Theta^+) \cdot \text{BR}(\Theta^+ \rightarrow pK_S^0)}{\sigma(K^*(892)^+)} &= \frac{Y(\Theta^+) \cdot \text{BR}(\Theta^+ \rightarrow pK_S^0) \cdot \epsilon_{K^*(892)^+}}{\epsilon_{\Theta^+ \rightarrow pK_S^0} \cdot Y(K^*(892)^+)} \\ \frac{\sigma(\Theta^+) \cdot \text{BR}(\Theta^+ \rightarrow pK_S^0)}{\sigma(\Sigma^*(1385)^\pm)} &= \frac{Y(\Theta^+) \cdot \text{BR}(\Theta^+ \rightarrow pK_S^0) \cdot \epsilon_{\Sigma^*(1385)^\pm}}{\epsilon_{\Theta^+ \rightarrow pK_S^0} \cdot Y(\Sigma^*(1385)^\pm)} \end{aligned} \quad (2)$$

All of the efficiencies include the reconstruction and selection efficiencies plus



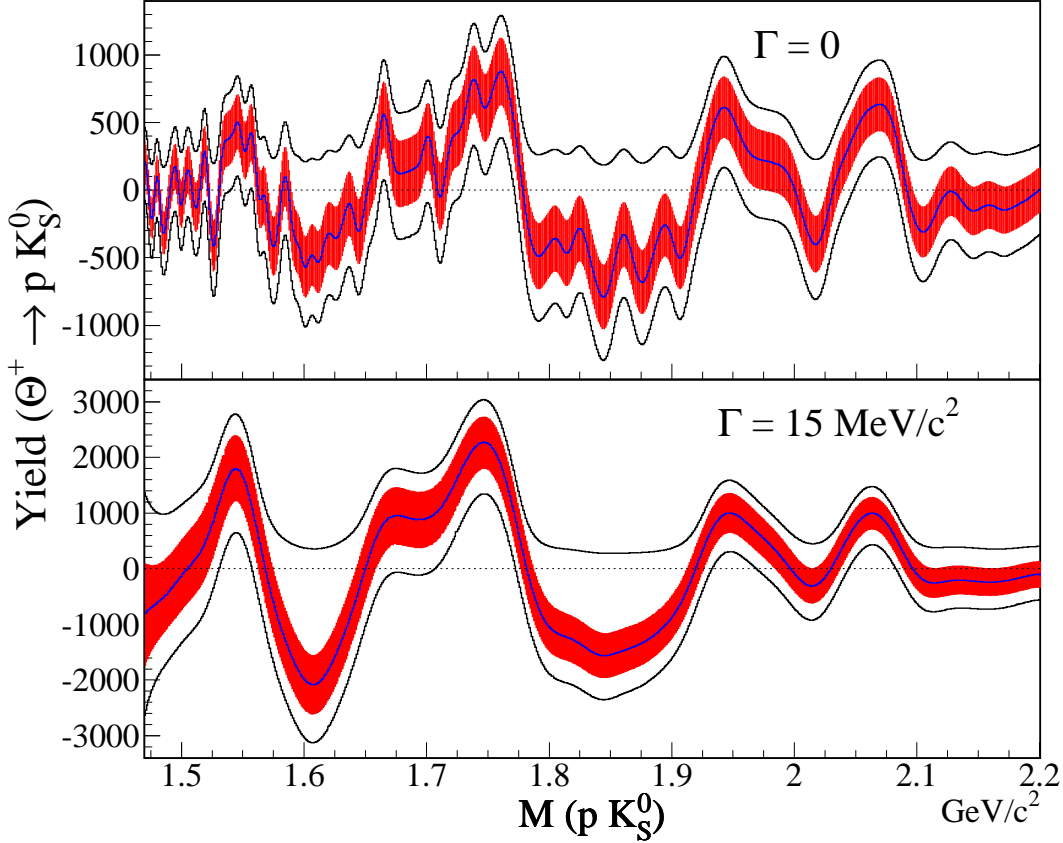


Fig. 7. Pentaquark yields and upper limits. Top (bottom) plots show results for a natural width of 0 ( $15 \text{ MeV}/c^2$ ). The shaded region includes the  $1\sigma$  errors with the central value in the middle. The outer curves show the upper and lower limits.

corrections for unseen decays of parent particles. The  $\Theta^+ \rightarrow pK_S^0$  efficiency only includes the correction for the unseen  $K_S^0$  decays, not corrections for  $\Theta^+ \rightarrow pK_L^0$  or other  $\Theta^+$  decay modes such as  $\Theta^+ \rightarrow nK^+$ . The  $K^*(892)^+$  and  $\Sigma^*(1385)$  efficiencies include all branching ratio corrections from the PDG [32]. For  $K^*(892)^+$  this corrections comes from  $\text{BR}(K_S^0 \rightarrow \pi^+\pi^-) = 0.6861$ ,  $\text{BR}(K^0 \rightarrow K_S^0) = 0.5$ , and  $\text{BR}(K^*(892)^+ \rightarrow \bar{K}^0\pi^+) = 0.667$  while for  $\Sigma^*(1385)^\pm$  the relevant branching ratios are  $\text{BR}(\Lambda^0 \rightarrow p\pi^-) = 0.64$  and  $\text{BR}(\Sigma^*(1385)^\pm \rightarrow \Lambda^0\pi^\pm) = 0.88$ . Determining reconstruction and selection efficiency (including acceptance) is described below.

The FOCUS detector is a forward spectrometer and therefore acceptance depends on the produced particle momentum. The production characteristics of the pentaquark are the largest sources of systematic uncertainty in this analysis. We choose a particular production model to obtain limits and provide sufficient information about the experiment for other interested parties to obtain limits based on other production models. The production simulation begins with a library of  $e^-$  and  $e^+$  tracks obtained from a TURTLE simulation [33] of the Wideband beam line. From this library, an individual track is drawn and bremsstrahlung photons created by passage through a

20%  $X_0$  lead radiator. Photons with energy above 15 GeV are passed to the PYTHIA [34] Monte Carlo simulation. The PYTHIA simulation is run using minimum bias events (MSEL=2) with varying energies (MSTP(171)=1). Options controlling parton distributions and gluon fragmentation were set to avoid heavy quark production (MSTP(58)=3 and MDME(156--160,1)=0). Also the center-of-mass minimum energy cut off was reduced from 10 GeV to 3 GeV (PARP(2)=3). However, the minimum photon energy requirement gives an effective minimum center-of-mass energy of 5.3 GeV. Since PYTHIA does not produce pentaquarks, another particle must be chosen to represent the pentaquark. Other than mass, the most important effect on the production is the number of quarks a particle has in common with the initially interacting hadrons, due to the nature of the PYTHIA string fragmentation model. The  $\Xi^*(1530)^0$  and  $\Sigma^*(1385)^+$  particles are chosen to represent the extremes in the production of a pentaquark. The  $\Xi^{*0}(ssu)$  ( $\Sigma^+(suu)$ ) can obtain at most 33% (67%) of the remaining quarks from the target nucleon valence quarks, while the  $\Theta^+(\bar{s}uudd)$  can take 60%. In all cases, the charge conjugate particles must obtain all quarks from the vacuum. The mass of the particle chosen to represent the pentaquark,  $\Xi^*(1530)^0$  or  $\Sigma^*(1385)^+$ , is set to the appropriate value in PYTHIA, by setting PMAS(190,1) or PMAS(187,1), respectively.

To calculate the relative cross sections in Eq. 2 we need efficiencies for  $\Sigma^*(1385)^\pm \rightarrow \Lambda^0 \pi^\pm$ ,  $K^*(892)^+ \rightarrow K_S^0 \pi^+$ , and  $\Theta^+ \rightarrow p K_S^0$ . These efficiencies are obtained from the FOCUS Monte Carlo simulation. The dominant uncertainty in the efficiency determination is the modeling of the production characteristics of the parent particle. For the observed particles,  $\Sigma^*(1385)^\pm$  and  $K^*(892)^+$ , we can compare the data and Monte Carlo directly and adjust the Monte Carlo simulation to produce the correct data distribution. Even this is not sufficient, however, because areas where the efficiency is zero cannot be accounted for. For  $\Sigma^*(1385)^\pm$  and  $K^*(892)^+$ , we run a weighted Monte Carlo simulation which matches the Monte Carlo momentum distribution with the observed data momentum distribution in the region for which the acceptance is not zero. The dominant source of uncertainty for the  $\Sigma^*(1385)^\pm \rightarrow \Lambda \pi^\pm$  and  $K^*(892)^+ \rightarrow K_S^0 \pi^+$  efficiencies is the our lack of knowledge of the fraction of events completely outside of our acceptance (momentum less than 15 GeV/c). The weighted PYTHIA Monte Carlo predicts 67% (79%) of the  $K^*(892)^+$  ( $\Sigma^*(1385)^\pm$ ) particles are produced with momentum less than 15 GeV/c. To obtain an estimate of the efficiency uncertainty, we assume that the number of particles with momentum less than 15 GeV/c can be off by up to a factor of 2 (high or low). This leads to a relative uncertainty on the  $K^*(892)^+$  and  $\Sigma^*(1385)^\pm$  efficiency of 43% and 49%, respectively. The  $\Theta^+ \rightarrow p K_S^0$  efficiency is taken as the average of the efficiencies obtained from using  $\Sigma^*(1385)^+$  and  $\Xi^*(1530)^0$  as the substitute particle while the uncertainty is half the difference between the two efficiencies. The  $\Theta^+ \rightarrow p K_S^0$  with  $K_S^0 \rightarrow \pi^+ \pi^-$  efficiency versus mass (with no branching ratio corrections) is shown in Fig. 8. The average uncertainty in  $\epsilon_{\Theta^+ \rightarrow p K_S^0}$  is approximately 26%. It may seem incongruous

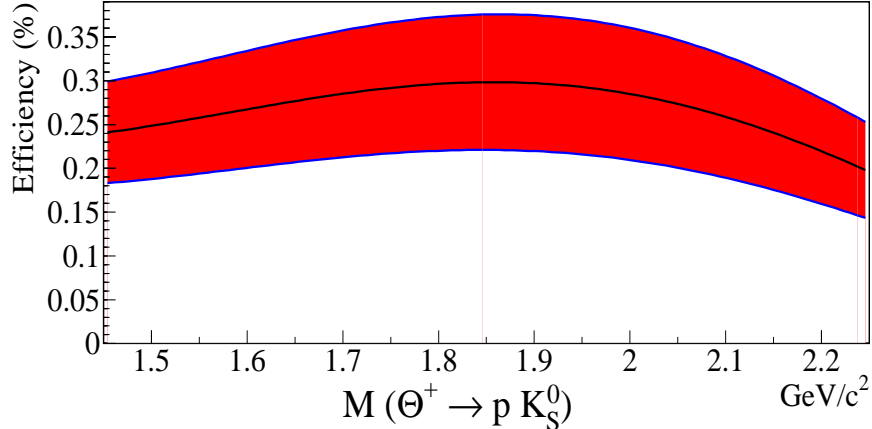


Fig. 8. Acceptance versus mass for pentaquark candidates. Upper (lower) curve is for a pentaquark produced as a  $\Xi^*(1530)^0$  ( $\Sigma^*(1385)^+$ ) and the middle is the average.

that the relative uncertainty of the efficiency of an unknown particle ( $\sim 26\%$ ) is less than that for the high statistics normalizing modes ( $>40\%$ ). The efficiency uncertainty of the high statistics modes reflects the lack of knowledge of production outside of our acceptance. However, it is reasonable to assume that discrepancies in the Monte Carlo simulation will be similar for the signal mode and the normalizing mode and therefore adding the uncertainty to the signal mode is double-counting. Note that the signal and normalizing efficiencies only appear as a ratio.

We also report the relative cross sections in the region where our acceptance is good, that is for parent particle momenta greater than  $25 \text{ GeV}/c$ . This dramatically reduces the systematic uncertainties associated with the measurement. The uncertainty due to the production of  $\Sigma^*(1385)^\pm$  and  $K^*(892)^0$  is minimal. The uncertainty in the  $\Theta^+$  efficiency is also dramatically reduced from approximately  $26\%$  to about  $6\%$  as shown in Fig. 9. The number of reconstructed  $K^*(892)^0$ ,  $\Sigma^*(1385)^+$ , and  $\Sigma^*(1385)^-$  at momenta greater than  $25 \text{ GeV}/c$  is 7.88 million, 127,000, and 212,000, respectively compared to the total sample of 8.98 million, 151,000, and 256,000, respectively with no momentum cut.

The upper limit on the yield was obtained by mathematically integrating the likelihood function from 0 to  $\infty$  and then integrating from 0 to 95% of the total likelihood integral gave the 95% CL upper limit. To obtain the limit on cross section requires a different approach due to the significant systematic uncertainties. We use a method based on a note by Convery [35] which is inspired by the Cousins and Highland [36] philosophy for including systematic uncertainties. Modifications to the Convery approach are made to give an exact solution [37].

Before systematics are considered, an analysis using a maximum likelihood fit returns a central value for the branching ratio ( $\hat{B}$ ) and a statistical error ( $\sigma_B$ ).

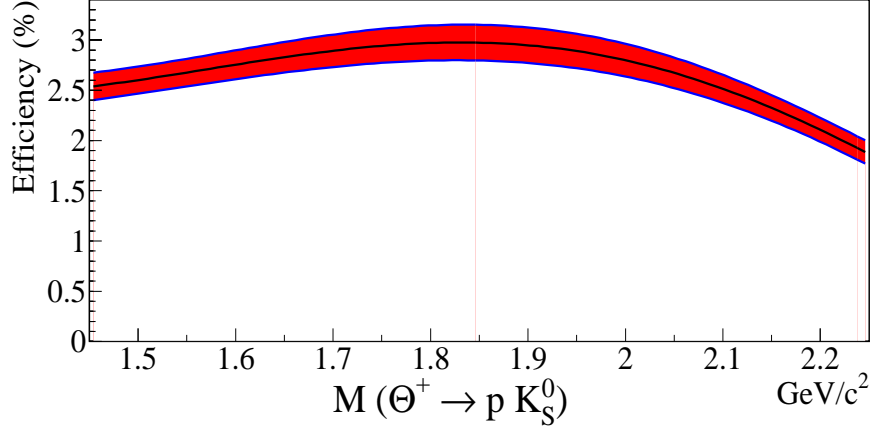


Fig. 9. Acceptance versus mass for pentaquark candidates. Lower (upper) curve is for a pentaquark produced as a  $\Xi^*(1530)^0$  ( $\Sigma^*(1385)^+$ ) and the middle is the average. The pentaquark is produced and reconstructed with momentum greater than 25 GeV/c.

The likelihood function is

$$p(B) \propto \exp\left[\frac{-(B - \hat{B})^2}{2\sigma_B^2}\right] \quad (3)$$

Following the notation in Convery, we associate  $\hat{S}$  with the nominal efficiency and  $\sigma_S$  as the error on the efficiency. Adding the uncertainty on the efficiency changes the likelihood to:

$$p(B) \propto \int_0^1 \exp\left[\frac{-(SB/\hat{S} - \hat{B})^2}{2\sigma_B^2}\right] \exp\left[\frac{-(S - \hat{S})^2}{2\sigma_s^2}\right] dS \quad (4)$$

Using Mathematica<sup>®</sup>, removing unimportant multiplicative constants, and changing variables from  $\sigma_S$  to  $\sigma_\epsilon \equiv \sigma_S/\hat{S}$ , the integral in Eq. 4 becomes:

$$p(B) \propto \frac{1}{\sqrt{\frac{B^2}{\sigma_B^2} + \frac{1}{\sigma_\epsilon^2}}} \exp\left[\frac{-(B - \hat{B})^2}{2(B^2\sigma_\epsilon^2 + \sigma_B^2)}\right] \left\{ \operatorname{erf}\left[\frac{B\hat{B}\sigma_\epsilon^2 + \sigma_B^2}{\sqrt{2}\sigma_\epsilon\sigma_B\sqrt{B^2\sigma_\epsilon^2 + \sigma_B^2}}\right] - \operatorname{erf}\left[\frac{(\hat{S} - 1)\sigma_B^2 - B\sigma_\epsilon^2(B - \hat{B}\hat{S})}{\sqrt{2}\hat{S}\sigma_\epsilon\sigma_B\sqrt{B^2\sigma_\epsilon^2 + \sigma_B^2}}\right] \right\} \quad (5)$$

We integrate Eq. 5 from 0 to  $\infty$  to obtain the total probability and then integrate from 0 to the point at which 95% of the total probability is included and define this as our 95% CL upper limit. The branching ratio  $B$  of Eq. 5 is simply the relative cross sections times the unknown pentaquark branching ratio as in Eq. 2. The relative uncertainties on the efficiency for the signal and normalizing mode are added in quadrature to become  $\sigma_\epsilon$  in Eq. 5. Furthermore,  $\hat{S}$  is the relative efficiency between the signal and normalizing modes and  $\sigma_B$  is

the statistical uncertainty on the branching ratio due simply to the uncertainty in the signal yield.

Figure 10 shows the results for  $\frac{\sigma(\Theta^+) \cdot \text{BR}(\Theta^+ \rightarrow p K_S^0)}{\sigma(K^*(892)^+)}$  with an assumed natural width of 0 (15) MeV/c<sup>2</sup> for the top (bottom) plot. This is the result corrected for all undetected particles. The shaded band shows the  $\pm 1\sigma$  limits with statistical uncertainties only; the line in the middle of the band is the central value. The top curve shows the 95% CL upper limit using the method described above including statistical and systematic uncertainties. The curve between the full upper limit and the  $1\sigma$  band is the 95% CL upper limit using the method described above with no systematic uncertainties included. The large systematic uncertainties are due to the attempt to correct for the vast majority of particles outside of our acceptance. While this systematic uncertainty significantly degrades the limit, the production times branching ratio of the pentaquark relative to  $K^*(892)^+$  production is still less than 0.0013 (0.0032) (95% CL) over the entire mass range for a natural width of 0 (15) MeV/c<sup>2</sup>. Figure 11 gives the same results for  $\frac{\sigma(\Theta^+) \cdot \text{BR}(\Theta^+ \rightarrow p K_S^0)}{\sigma(\Sigma^*(1385)^\pm)}$ . In this case, the 95% CL upper limit on the pentaquark production times branching ratio relative to  $\Sigma^*(1385)^\pm$  is 0.025 (0.062) over the entire mass range for a natural width of 0 (15) MeV/c<sup>2</sup>.

Figures 12 and 13 show the same results for the restricted range of momentum greater than 25 GeV/c. That is, they show limits on relative cross sections for particles ( $\Theta^+$ ,  $K^*(892)^+$ ,  $\Sigma^*(1385)^\pm$ ) produced with  $p > 25$  GeV/c.

## 4 Conclusions

We find no evidence for pentaquarks decaying to  $p K_S^0$  in the mass range of 1470 MeV/c<sup>2</sup> to 2200 MeV/c<sup>2</sup>. In contrast, we observe 9 million  $K^*(892)^+ \rightarrow K_S^0 \pi^+$  particles and 0.4 million  $\Sigma^*(1385)^\pm \rightarrow \Lambda^0 \pi^\pm$  particles which have a very similar topology and energy release. We set 95% CL upper limits on the yield over the entire mass range with a maximum of 1300 (3000) events for an assumed natural width of 0 (15) MeV/c<sup>2</sup>. We also obtain 95% CL upper limits on the cross section for pentaquark production times the branching ratio to  $p K_S^0$  relative to  $K^*(892)^+ \rightarrow K_S^0 \pi^+$  and  $\Sigma^*(1385)^\pm \rightarrow \Lambda^0 \pi^\pm$ . These limits are determined for two cases. The first case is for parent particles produced at any momenta (albeit with a minimum center-of-mass energy of 5.3 GeV) where we find a maximum upper limit of  $\frac{\sigma(\Theta^+) \cdot \text{BR}(\Theta^+ \rightarrow p K_S^0)}{\sigma(K^*(892)^+)} < 0.0013$  (0.0033) and  $\frac{\sigma(\Theta^+) \cdot \text{BR}(\Theta^+ \rightarrow p K_S^0)}{\sigma(\Sigma^*(1385)^\pm)} < 0.023$  (0.057) at 95% CL for a natural width of 0 (15) MeV/c<sup>2</sup>. In the second case we measure the relative cross sections for parent particles with momenta above 25 GeV/c (a region of good acceptance)

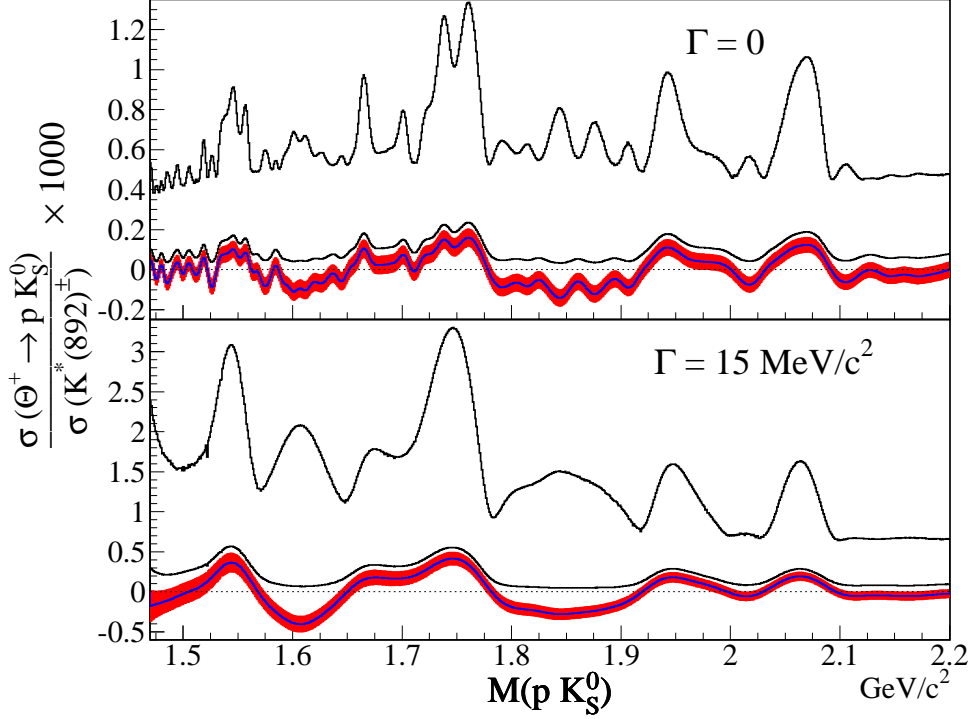


Fig. 10.  $\frac{\sigma(\Theta^+) \times \text{BR}(\Theta^+ \rightarrow p K_S^0)}{\sigma(K^*(892)^+)}$  versus mass. Top (bottom) plots show results for a  $\Theta^+$  natural width of 0 ( $15 \text{ MeV}/c^2$ ). The shaded region encompasses the  $1\sigma$  statistical uncertainty with the central value in the middle. The top curve shows the 95% CL upper limit including systematic uncertainties while the middle curve is the 95% CL upper limit with statistical uncertainties only.

and calculate 95% CL limits of  $\frac{\sigma(\Theta^+) \cdot \text{BR}(\Theta^+ \rightarrow p K_S^0)}{\sigma(K^*(892)^+)} < 0.00012$  (0.00029) and  $\frac{\sigma(\Theta^+) \cdot \text{BR}(\Theta^+ \rightarrow p K_S^0)}{\sigma(\Sigma^*(1385)^\pm)} < 0.0042$  (0.0099) for a natural width of 0 ( $15 \text{ MeV}/c^2$ ).

Very few of the observing experiments report results for  $K^*(892)^+ \rightarrow K_S^0 \pi^+$  and  $\Sigma^*(1385)^\pm \rightarrow \Lambda^0 \pi^\pm$  yields. One CLAS result apparently finds a yield of  $\sim 1000 K^*(892)^+$  [38] while SVD reconstructs  $\sim 125 K^*(892)^+ \rightarrow K_S^0 \pi^+$  and  $\sim 100 \Sigma^*(1385)^+ \rightarrow \Lambda^0 \pi^+$  decays [10]. The FOCUS results presented here represent samples that are more than 2000 times larger. Unfortunately, differences in production between (mostly) low energy experiments which have reported observations and a high energy experiment such as FOCUS prevent any definitive conclusions from being drawn.

## 5 Acknowledgments

We wish to acknowledge the assistance of the staffs of Fermi National Accelerator Laboratory, the INFN of Italy, and the physics departments of the collaborating institutions. This research was supported in part by the U. S.

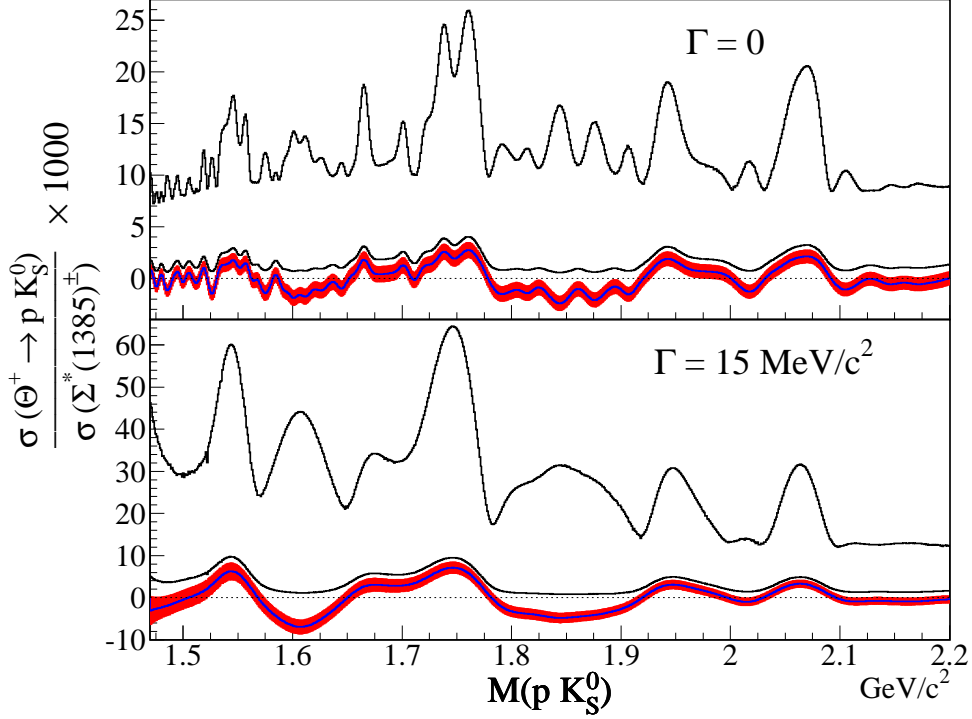


Fig. 11.  $\frac{\sigma(\Theta^+) \times \text{BR}(\Theta^+ \rightarrow p K_S^0)}{\sigma(\Sigma^*(1385)^+) + \sigma(\Sigma^*(1385)^-)}$  versus mass. Top (bottom) plots show results for a  $\Theta^+$  natural width of 0 ( $15 \text{ MeV}/c^2$ ). The shaded region encompasses the  $1 \sigma$  statistical uncertainty with the central value in the middle. The top curve shows the 95% CL upper limit including systematic uncertainties while the middle curve is the 95% CL upper limit with statistical uncertainties only.

National Science Foundation, the U. S. Department of Energy, the Italian Istituto Nazionale di Fisica Nucleare and Ministero dell'Istruzione dell'Università e della Ricerca, the Brazilian Conselho Nacional de Desenvolvimento Científico e Tecnológico, CONACyT-México, the Korean Ministry of Education, and the Korean Science and Engineering Foundation.

## References

- [1] R. L. Jaffe, Phys. Rev. D 15 (1977) 267; R. L. Jaffe, Phys. Rev. D 15 (1977) 281; R. L. Jaffe, Phys. Rev. Lett. 38 (1977) 195; Erratum-ibid 38 (1977) 617.
- [2] A. Chodos et al., Phys. Rev. D 9 (1974) 3471; T. DeGrand et al., Phys. Rev. D 12 (1975) 2060.
- [3] T. Nakano et al. [LEPS Collaboration], Phys. Rev. Lett. 91 (2003) 012002.
- [4] V. V. Barmin et al. [DIANA Collaboration], Phys. Atom. Nucl. 66 (2003) 1715.
- [5] S. Stepanyan et al. [CLAS Collaboration], Phys. Rev. Lett. 91 (2003) 252001.
- [6] J. Barth et al. [SAPHIR Collaboration], Phys. Lett. B 572 (2003) 127.

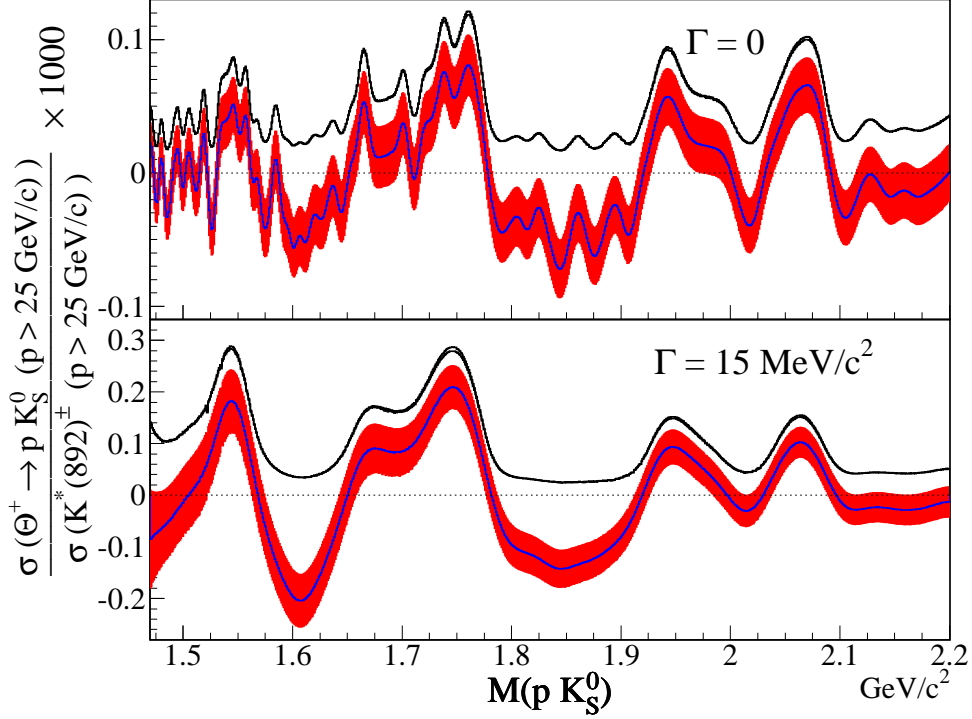


Fig. 12.  $\frac{\sigma(\Theta^+ \rightarrow p K_S^0) \times \text{BR}(\Theta^+ \rightarrow p K_S^0)}{\sigma(K^*(892)^+)}$  for  $p > 25 \text{ GeV}/c$  versus mass. Top (bottom) plots show results for a  $\Theta^+$  natural width of 0 ( $15 \text{ MeV}/c^2$ ). The shaded region encompasses the  $1\sigma$  statistical uncertainty with the central value in the middle. The top curve shows the 95% CL upper limit including systematic uncertainties and is virtually indistinguishable from the middle curve which shows the 95% CL upper limit with statistical uncertainties only.

- [7] A. E. Asratyan et al., Phys. Atom. Nucl. 67 (2004) 682.
- [8] V. Kubarovsky et al. [CLAS Collaboration], Phys. Rev. Lett. 92 (2004) 032001; Erratum-ibid. 92 (2004) 049902.
- [9] A. Airapetian et al. [HERMES Collaboration], Phys. Lett. B 585 (2004) 213.
- [10] A. Aleev et al. [SVD Collaboration], Phys. Atom. Nucl. 68 (2005) 974.
- [11] M. Abdel-Bary et al. [COSY-TOF Collaboration], Phys. Lett. B 595 (2004) 127.
- [12] S. Chekanov et al. [ZEUS Collaboration], Phys. Lett. B 591 (2004) 7.
- [13] D. Diakonov, V. Petrov, and M. V. Polyakov, Z. Phys. A 359 (1997) 305.
- [14] C. Alt et al. [NA49 Collaboration], Phys. Rev. Lett. 92 (2004) 042003.
- [15] A. Aktas et al. [H1 Collaboration], Phys. Lett. B 588 (2004) 17.
- [16] S. Schael et al. [ALEPH Collaboration], Phys. Lett. B 599 (2004) 1.
- [17] B. Aubert et al. [BABAR Collaboration], Phys. Rev. Lett. 95 (2005) 042002.
- [18] R. Mizuk et al. [Belle Collaboration], Phys. Lett. B 632 (2006) 173.



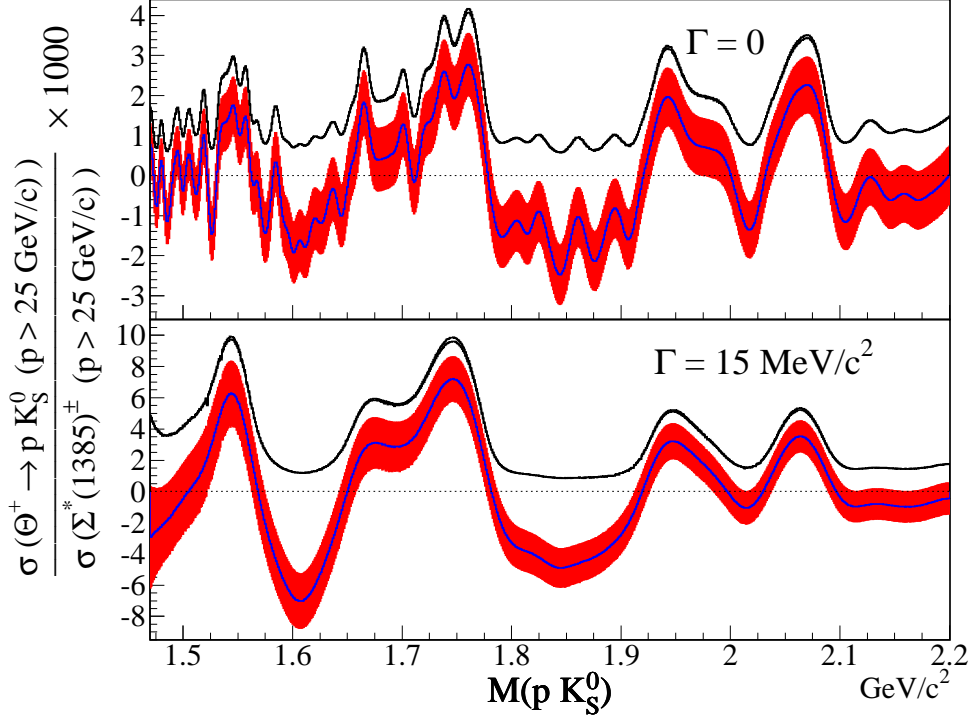


Fig. 13.  $\frac{\sigma(\Theta^+) \times \text{BR}(\Theta^+ \rightarrow p K_S^0)}{\sigma(\Sigma^*(1385)^+) + \sigma(\Sigma^*(1385)^-)}$  for  $p > 25 \text{ GeV}/c$  versus mass. Top (bottom) plots show results for a  $\Theta^+$  natural width of 0 ( $15 \text{ MeV}/c^2$ ). The shaded region encompasses the  $1\sigma$  statistical uncertainty with the central value in the middle. The top curve shows the 95% CL upper limit including systematic uncertainties and is virtually indistinguishable from the middle curve which shows the 95% CL upper limit with statistical uncertainties only.

- [19] J. Z. Bai et al. [BES Collaboration], Phys. Rev. D 70 (2004) 012004.
- [20] I. V. Gorelov [CDF Collaboration], arXiv:hep-ex/0408025; D. O. Litvintsev [CDF Collaboration], Nucl. Phys. Proc. Suppl. 142 (2005) 374.
- [21] I. Abt et al. [HERA-B Collaboration], Phys. Rev. Lett. 93 (2004) 212003.
- [22] M. J. Longo et al. [HyperCP Collaboration], Phys. Rev. D 70 (2004) 111101.
- [23] J. Napolitano, J. Cummings, and M. Witkowski, arXiv:hep-ex/0412031.
- [24] S. R. Armstrong [LEP], Nucl. Phys. Proc. Suppl. 142 (2005) 364.
- [25] C. Pinkenburg [PHENIX Collaboration], J. Phys. G 30 (2004) S1201.
- [26] Y. M. Antipov et al. [SPHINX Collaboration], Eur. Phys. J. A 21 (2004) 455.
- [27] M. Battaglieri et al. [CLAS Collaboration], Phys. Rev. Lett. 96 (2006) 042001.
- [28] J. M. Link et al. [FOCUS Collaboration], Nucl. Instrum. and Meth. A 516 (2004) 364.
- [29] J. M. Link et al. [FOCUS Collaboration], Nucl. Instrum. and Meth. A 484 (2002) 174.

- [30] J. M. Link et al. [FOCUS Collaboration], Nucl. Instrum. and Meth. A 484 (2002) 270.
- [31] F. James and CN/ASD Group, MINUIT - Function Minimization and Error Analysis – Reference Manual, Version 94.1, CERN (1994), unpublished.
- [32] S. Eidelman et al. [Particle Data Group], Phys. Lett. B 592 (2004) 1.
- [33] D. C. Carey et al., Decay TURTLE (Trace Unlimited Rays Through Lumped Elements): A Computer Program for Simulating Charged Particle Beam Transport Systems, Including Decay Calculations, SLAC-R-246, FERMILAB-PM-31, (1982), unpublished.
- [34] T. Sjöstrand, Comp. Phys. Comm. 101 (1994) 232.
- [35] M. R. Convery, Incorporating Multiplicative Systematic Errors in Branching Ratio Limits, SLAC-TN-03-001, 2003.
- [36] R. D. Cousins and V. L. Highland, Nucl. Instrum. and Meth. A320 (1992) 331.
- [37] K. Stenson, arXiv:physics/0605236.
- [38] L. Guo, D. P. Weygand, V. Kubarovsky [CLAS Collaboration], J. Phys. Conf. Ser. 9 (2005) 272.